INTERFACE

rsif.royalsocietypublishing.org

Research

Cite this article: Potomkin M, Tournus M, Berlyand LV, Aranson IS. 2017 Flagella bending affects macroscopic properties of bacterial suspensions. *J. R. Soc. Interface* **14**: 20161031. http://dx.doi.org/10.1098/rsif.2016.1031

Received: 19 December 2016
Accepted: 3 May 2017

Subject Category:
Life Sciences–Physics interface

Subject Areas:
biomathematics, biophysics

Keywords:
microswimmers, flagellum, effective viscosity, bacterial suspension, bacteria–surface interactions

Author for correspondence:
I. S. Aranson
e-mail: aronson@anl.gov

Electronic supplementary material is available online at https://dx.doi.org/10.6084/m9.figshare.c.3780107.

THE ROYAL SOCIETY PUBLISHING

Flagella bending affects macroscopic properties of bacterial suspensions

M. Potomkin[1], M. Tournus[3], L. V. Berlyand[1] and I. S. Aranson[1,2,4]

[1]Department of Mathematics, and [2]Department of Biomedical Engineering, Pennsylvania State University, University Park, PA 16802, USA
[3]Aix Marseille Univ, CNRS, Centrale Marseille, I2M, Marseille, France
[4]Materials Science Division, Argonne National Laboratory, 9700 South Cass Avenue, Argonne, IL 60439, USA

ISA, 0000-0002-4062-5393

To survive in harsh conditions, motile bacteria swim in complex environments and respond to the surrounding flow. Here, we develop a mathematical model describing how flagella bending affects macroscopic properties of bacterial suspensions. First, we show how the flagella bending contributes to the decrease in the effective viscosity observed in dilute suspension. Our results do not impose tumbling (random reorientation) as was previously done to explain the viscosity reduction. Second, we demonstrate how a bacterium escapes from wall entrapment due to the self-induced buckling of flagella. Our results shed light on the role of flexible bacterial flagella in interactions of bacteria with shear flow and walls or obstacles.

1. Introduction

Bacteria, being among the simplest living organisms, are the most abundant species on the planet. They significantly influence carbon cycling and sequestration, decomposition of biomass and transformation of contaminants in the environment. Trillions of symbiotic and pathogenic bacteria share human body space and form microbiota. Behaviour of bacterial suspensions is an active topic of research [1–6]. The recent discoveries include the onset of large-scale collective behaviour [2,3,7,8], reduction of effective viscosity [9–11], rectification of random motion of bacteria and extraction of useful energy [12–14], and enhanced mixing in bacterial suspensions [1,15–17].

Some motile bacteria utilize bundled helical flagella to propel themselves in a fluid environment. Bacteria use the propensity to swim to search for food (e.g. chemotaxis), colonize new territory or escape harsh conditions. Orientation of bacteria is also affected by shear flow, leading to a variety of non-trivial effects, such as rheotaxis (swimming against the flow) [18] or depletion of bacterial concentration in shear flows [5,19]. Unlike chemotaxis, i.e. drift along the concentration gradient, rheotaxis and concentration depletion are purely physical effects since no active receptor response is needed for the explanation of these phenomena. Elastomechanics of the bacteria, like bending and buckling of the flagella, could then play an important role in the understanding of these phenomena [20]. A flagellum is, typically, at least twice longer than the bacterial body and is flexible. Thus, flagellar bending could result in a significant effect on bacterial trajectories [20–23]. Nonlinear dynamics of rigid microswimmers in two-dimensional Poiseuille flow were studied in [24,25]. It was shown that the swimmers initially located away from channel walls exhibit a stable periodic motion around the centreline of the flow. The role of bacteria motility in zipping of individual flagellar filaments and the formation of the bacteria flagella bundle was investigated in [26]. However, it was poorly understood how the flagellum can affect the bacterial dynamics due to bending in response to the external shear flow or due to collision with the wall or obstacle. A model of a swimmer with flexible flagella in two fundamental shear flows, either planar shear or Poiseuille flow in long channels, has been introduced in our previous work [27]. A variety of surprising effects was discovered.

For example, depending on the bending stiffness of the flagellum, the swimmer may migrate towards the centre or exhibit periodic motion. This paper significantly extends and advances our results obtained in [27]. Here, we succeed in tackling two new important problems associated with the bacterial dynamics in shear flows. We show that flexibility of the bacterial flagella (i) contributes to the reduction of the effective viscosity and (ii) assists bacteria escaping entrapment near solid walls. Our results provide insight on how microswimmers interact with external shear flow and with obstacles, realized, for example, in microfluidic devices or *in vivo*.

The first part of this work is motivated by the experimental observation in [9,10] on the decrease of the effective viscosity of an active suspension of *B. subtilis*, in particular in the dilute regime, that is, when the volume fraction of bacteria is less than 1%. This result has been recently extended in [11] where a suspension of *E. coli* exhibited properties reminiscent of those of a super fluid: persistent flow and zero (or even negative) apparent viscosity. This is a hallmark of active matter: chemical energy stored in nutrients is turned into mechanical energy which is then used to counter-balance the viscous dissipation. Suspensions of active (self-propelled) swimmers representing bacteria were studied in [19,28–30] with the primary goal to identify a mechanism resulting in the decrease of effective viscosity in a dilute regime. The works [28–30] require bacteria to tumble (randomly change direction characterized by some tumbling rate or effective rotational diffusion D_r). Nevertheless, the strain of *B. subtilis* used in [9] tumbles rarely, i.e. $D_r \ll 1$. Here, we show that bacterial flagella bending contributes to the reduction of the effective viscosity even in the absence of tumbling. We derive an asymptotic expression for the effective viscosity for a dilute suspension. We show that this expression is in agreement with both the numerical solution of the model and qualitatively consistent with the experimental data from [9].

The second part of the work focused on the bacterial behaviour near surfaces (e.g. obstacles or walls). Swimming of bacteria in the presence of walls is important for the macroscopic properties of suspensions since these properties depend significantly on the spatial distribution of bacteria. The problem of the bacterial behaviour near surfaces naturally occurs in multiple settings relevant in the biomedical context (formation of biofilms, migration of bacteria along channels, e.g. catheter) and industry (pipes clogging, biofouling). In many situations, bacteria swim in a confined container and their trajectory can be significantly affected by a nearby surface. Typically, bacteria are attracted by a no-slip surface (a wall) due to long-range hydrodynamic interactions [31], and then swim (mostly) parallel to the wall for a certain period of time. Eventually, bacteria can escape due to tumbling [4] or can permanently adhere to the wall. Study of the behaviour of flagellated swimmers near walls was initiated by [32] where the accumulation of spermatozoa at glass plates was documented. In the experimental works [33,34] it was shown that *E. coli* is attracted by the wall and the straight trajectory becomes circular due to counter-rotation of the bacterial body and the flagella. The tendency of bacteria to approach the wall and to increase the curvature of their trajectory was observed by numerical modelling in [35] where a bacterium was modelled as a sphere with a helical flagellum rotating with constant angular velocity. To explain why the bacteria can swim near the wall adjacent to it for a long time, in [36] the authors hypothesized the presence of short-ranged forces of van der Waals type. However, in [37], by combining theory and experiment, it was shown that van der Waals forces cannot be responsible for parallel swimming of the bacteria near the wall. Instead authors proposed to extend the model from [35] for a non-spherical bacterium body, and showed that bacteria may be kept at the wall by the additional torque caused by the non-sphericity. In addition to hydrodynamic attraction, bacteria can eventually reorient themselves and swim away from the wall (escape). In [4], the time needed for bacteria to escape was estimated theoretically, provided that rotational diffusion (for example, due to tumbling) is introduced. Drecher *et al*. [4] noted that even if bacteria do not tumble and are too large to be affected by thermal effects, the rotational diffusion can be assigned with a significant value due to noise in the swimming mechanism, whose essential constituent is flagella dynamics.

Here, we consider how a flagellated bacterium, being initially entrapped and immobilized at a wall, can escape by exploiting the flexibility of its flagella. Such an entrapment may also naturally happen when the suspending liquid is anisotropic, e.g. lyotropic liquid crystal [38,39]. In this situation, bacteria are swimming predominantly parallel to the average molecular orientation, i.e. liquid crystal director. In the case when the liquid crystal director is anchored perpendicular to the confining wall (homeotropic alignment), bacteria are forced to be aligned perpendicular to the wall and become trapped [38,40]. When the motility of bacteria is increased (by adding oxygen), the bacterium may turn parallel to the wall due to the torque coming from the wall. Also, the forces which kept bacteria immobilized are small in comparison to the propulsion force (weak surface anchoring of the liquid crystal molecules). We show that a bacterium with rigid flagellum swims along the wall, so it stays essentially entrapped. By contrast, we show that a bacterium with flexible flagellum may rotate by an angle larger than $\pi/2$ and escape. An ability to escape from the wall is important for macroscopic properties of suspensions since it affects accumulation of bacteria at the wall, and thus distribution of bacteria in the whole domain. For example, effective viscosity is a function of the spatial distribution of bacteria. Thus, wall accumulation will affect the spatial distribution of bacteria, and, correspondingly, will contribute to the apparent viscosity.

To obtain results of both parts, we extend the model from [27], referred to below as MMFS (the mathematical model of flagellated swimmer). The model is two-dimensional and describes the swimmer as a rigid elliptic body (major and minor axes are denoted by ℓ and d, respectively) with an attached elastic beam representing flagella (figure 1). The orientation of the swimmer θ_0 is defined as the orientation of the principal axis of the body with respect to the horizontal. The flagellum is a segment of a curve of constant length L and $\theta(s)$ is the tangential angle of the flagellum at the point corresponding to arc length parameter s, $0 \le s \le L$. The underlying physical assumptions of MMFS are outlined in §5. MMFS requires solving a coupled system of nonlinear differential equations that were obtained from the force and torque balances for the swimmer. This mathematical model, as well as balance equations, can be found in electronic supplementary material, S1.

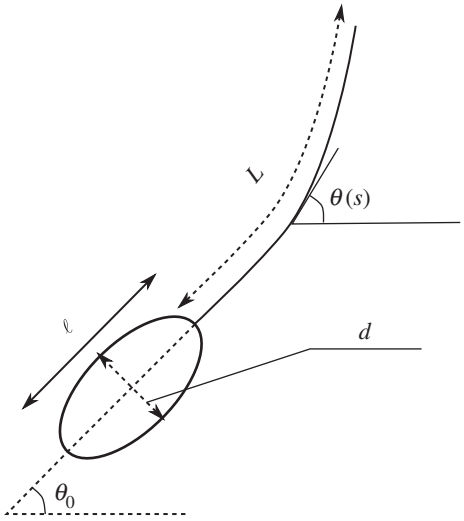

Figure 1. Schematics of the flagellated swimmer.

2. Results

2.1. Effective viscosity of a dilute suspension of flagellated swimmers

2.1.1. A general formula for effective viscosity

Effective viscosity can be understood as a measure of the total shear stress of a suspension induced by a prescribed shear flow. In the context of bacterial suspensions, the stress resulting from the applied strain is due to the intrinsic resistance of suspending fluid and due to the stress created by the microswimmers (bacteria). In the dilute regime, interactions between bacteria are negligible. Therefore, the superposition principle applies: the contribution to the total stress from all bacteria is the sum of the individual contributions. Moreover, due to their large number, each bacterium's contribution may be approximated in the sum by its expected value (taking a continuum limit). The dilute framework enables us to use MMFS to derive macroscopic properties of the suspension. The formula for the effective viscosity η_{eff} in a linear planar shear background flow of strain rate $\dot{\gamma}$ becomes [28,29,41–43]

$$\begin{aligned}\eta_{\text{eff}} &= \eta_0 + \sum_{i=1}^{n} \eta_{\text{bact},i} \\ &\approx \eta_0 + n\int_0^{2\pi} \frac{\Sigma_{12}(\theta_0) + \Sigma_{21}(\theta_0)}{2\dot{\gamma}} P(\theta_0)\,\mathrm{d}\theta_0, \end{aligned} \tag{2.1}$$

where η_0 is the viscosity of the suspending fluid, $n = \Phi V_L$ is the number of particles in the volume V_L occupied by a suspension, Φ is the number density of bacteria and $P(\theta_0)$ is the bacterial orientation probability distribution function. The integral in the r.h.s. of equation (2.1) is the expected value of the contribution to the effective viscosity $\eta_{\text{bact},i}$ of the ith bacterium. The effective viscosity $\eta_{\text{bact},i}$ is the ratio between the anti-diagonal components Σ_{12} and Σ_{21} of the stress tensor Σ (induced by the bacterium) and the applied shear rate $\dot{\gamma}$. Here, we assume that Σ_{12} and Σ_{21} are only determined by the orientation angle θ_0 of the bacterium. To compute the expected values of Σ_{12} and Σ_{21}, finding the distribution of orientation angles $P(\theta_0)$ is necessary.

MMFS is based on balance of forces and torques exerted by the swimmer and the fluid on the swimmer's rigid body and at each point of the flexible flagellum. The sum of forces exerted by the swimmer on the fluid is zero. This is similar to the force-dipole model of a swimmer [4,43] where the sum of the force that pushes the body in the fluid and the resistive (or viscous drag) force that perturbs the fluid due to the propulsion mechanism in the flagella (represented in the force-dipole model by a point force exerted behind the body) is zero. The key difference between MMFS and the force-dipole model is that the sum of all torques exerted by the swimmer in MMFS is not necessarily zero, whereas for force dipoles this sum is trivially zero. In particular, the force dipole cannot rotate if no external torque is exerted (a non-zero background flow, interactions with other swimmers, external magnetic field, etc.), while the flagellated swimmer may rotate if the flagellum is bent. The fact that the fluid balances a non-zero total torque exerted by the swimmer results, in general, in the effective stress being non-symmetric in MMFS, i.e. $\Sigma_{12} \neq \Sigma_{12}$ [44]. A non-zero anti-symmetric part of the effective stress due to active contribution is the special feature of active chiral fluids [45].

To find the stress tensor components Σ_{kl} one needs to solve the Stokes equation in the low Reynolds number regime: $-\nabla_{\mathbf{x}} \cdot \Sigma(\mathbf{x}) = F_{\text{bact}}(\mathbf{x})$, where Σ is the fluid stress tensor, and F_{bact} is the bulk force due to the presence of the bacterium (the thrust force). Solving this equation is impractical due to the large domain of integration compared with the bacterium size. In a simpler model of a bacterium with rigid flagellum [43], each bacterium was approximated by a force dipole [4] and the explicit expression for Σ is well known in this case. Here, our goal is to capture the effects coming from bending of elastic flagella in shear flow, so an approximation by the force dipole would oversimplify the consideration and would lead to zero net contribution to the effective viscosity. Instead, we use the Kirkwood approximation for the stress tensor [46–48]

$$\Sigma_{kl} = \frac{1}{V_L}\int (F_{\text{bact}}(\mathbf{x}))_k (\mathbf{x} - \mathbf{x}_c)_l \,\mathrm{d}\mathbf{x}, \tag{2.2}$$

where $F_{\text{bact}}(\mathbf{x})$ is non-zero in a small neighbourhood of the centre of mass of the bacterium $\mathbf{x}_c$, and V_L is the volume occupied by the fluid. The Kirkwood approximation can be also interpreted as the second term in the multipole expansion of the Stokes flow [42].

In the context of MMFS, $F_{\text{bact}}(\mathbf{x})$ is the sum of two forces distributed over the flagellum: (i) the uniform propulsion force $F_p \boldsymbol{\tau}(s)$ directed along the unit tangent vector $\boldsymbol{\tau}(s)$ with the magnitude F_p and (ii) the elastic force $Q(s) = \Lambda(s)\boldsymbol{\tau}(s) + N(s)\boldsymbol{n}(s)$ (Λ and N are tangent and normal components of Q, respectively). In the following, it will be convenient to separate contributions coming from propulsion and from elasticity for the components of the stress tensor: $\Sigma_{kl} = \Sigma_{kl}^{\text{propulsion}} + \Sigma_{kl}^{\text{elastic}}$, where according to equation (2.2)

$$\left.\begin{aligned} \Sigma_{kl}^{\text{propulsion}} &= \frac{1}{V_L}\int_0^L F_p \tau_k(s)(X_l(s) - X_l(0))\,\mathrm{d}s \\ \text{and} \qquad \Sigma_{kl}^{\text{elastic}} &= \frac{1}{V_L}\int_0^L \frac{\partial Q_k}{\partial s}(s)(X_l(s) - X_l(0))\,\mathrm{d}s, \end{aligned}\right\} \tag{2.3}$$

and analogously for the effective viscosity η_{eff}:

$$\eta_{\text{eff}} - \eta_0 = \eta_{\text{propulsion}} + \eta_{\text{elastic}}. \tag{2.4}$$

Terms $\eta_{\text{propulsion}}$ and η_{elastic} are computed via (2.3) and (2.1). They take into account the effect of the flagellum. This means

Table 1. Comparison of numerical solution with the asymptotic results.

	$K_b = 3\times10^{-23}$ N m^2		$K_b = 9\times10^{-23}$ N m^2	
	asymptotics	numerics	asymptotics	numerics
$\frac{\eta_{eff}-\eta_0}{\eta_0} < 0$	$L > 15$ μm	$L > 11$ μm	$L > 22$ μm	$L > 15$ μm
	$r < 0.33$	$r < 0.45$	$r < 0.23$	$r < 0.34$
	$\varepsilon > 0.16$	$\varepsilon > 0.05$	$\varepsilon > 0.24$	$\varepsilon > 0.05$
$\frac{\eta_{eff}-\eta_0}{\eta_0} < 10\%$	$L > 16$ μm	$L > 12$ μm	$L > 23$ μm	$L > 16$ μm
	$r < 0.31$	$r < 0.43$	$r < 0.22$	$r < 0.32$
	$\varepsilon > 0.21$	$\varepsilon > 0.06$	$\varepsilon > 0.26$	$\varepsilon > 0.06$

that the contribution to the effective viscosity due to the presence of rigid bodies in the fluid is included in η_0. In other words, η_0 is the effective viscosity of the dilute suspension of rigid bodies and $\eta_0 \approx \eta_{\text{fluid}}[1 + \nu\Phi]$, where η_{fluid} is the viscosity of water and Φ is the number density. The formula for the coefficient ν is well known: for spheres $\nu = 2.5$ (the Einstein formula [49]); for ellipsoids ν was obtained by Jeffery (formulas (62) and (64) in [50]).

2.1.2. Asymptotic results for large bending stiffness of flagellum

We present here our results on computations of $\eta_{\text{propulsion}}$ and η_{elastic} as functions of the following geometrical and physical dimensionless parameters: shape parameter β (describes the shape of the bacterium body; $\beta = 0$ for rods and 1/2 for spheres), ratio of bacterial body length to the flagella length $r = \ell/L$ (ℓ and L are the body and the flagellum length, respectively) and the compound dimensionless parameter characterizing ratio of drag force to elastic force $\varepsilon = L^4\dot{\gamma}\zeta_b/K_b$ (ζ_b is the drag coefficient and K_b is the bending stiffness of the flagellum). We use two scale asymptotic expansions in small ε (stiff flagella) to establish an explicit expression for the effective viscosity η_{eff}. Note that, for fixed values of ζ_b, L and $\dot{\gamma}$, taking ε small is equivalent to the flagellum being nearly rigid. This implies that the bending stiffness of the flagellum K_b is large (the reader should not be confused by the fact that the typical K_b we use for bacteria and call it 'large' is of the order of 10^{-23} N m^2; after non-dimensionalization K_b is replaced by ε^{-1}; for details see electronic supplementary material, S2). Necessity of two scales in the asymptotic expansions in the 'rigid' limit is explained by the two different time scales for the smoothly translating bacterial body and rapidly deforming flagellum.

The two-scale asymptotic expansion for equations of MMFS is used to derive the following asymptotic expression for the tangential and normal components of the elastic stress: $\Lambda(s) = p_\Lambda(s)\sin 2\theta_0 - F_p(s-L)/(1+k_r)$, $N(s) = p_N(s)\cos 2\theta_0$. Polynomials $p_\Lambda(s)$ and $p_N(s)$ are of second order with respect to arclength s with coefficients proportional to ζ_b and $\dot{\gamma}$ and they also depend on shape parameter β, flagellum length L, body length ℓ and drag coefficient k_r (see table 2 with the list of parameters). The second term in the expression for the tangential component of the elastic stress is due to the propulsion force which acts in the tangential direction $\boldsymbol{\tau}$ with the strength F_p. We also found the asymptotic expression for the flagellum shape described by the slope angle: $\theta(s) = \theta_0 + \varepsilon p_\theta(s)\cos 2\theta_0$, where $p_\theta(s)$ is a polynomial of fourth order with respect to arclength s and coefficients depending on β, ℓ, L, k_r. Details of derivation for Λ, N and θ with explicit formulas for coefficients of polynomials p_Λ, p_N and p_θ can be found in the electronic supplementary material.

The distribution of orientation angles $P(\theta_0)$ from equation (2.1) is in general a function of both angle of the body θ_0 and time t. It satisfies the Liouville continuity equation

$$\left.\begin{aligned} &\frac{\partial}{\partial t}P(\theta_0,t) + \frac{\partial}{\partial\theta_0}\left[\frac{T_{\text{shear}} + T_{\text{flagellum}}}{\zeta_r}P(\theta_0,t)\right] = 0 \\ \text{and}\quad &\int_0^{2\pi} P(\theta_0,t)\,d\theta_0 = 1, \end{aligned}\right\} \tag{2.5}$$

where T_{shear} and $T_{\text{flagellum}}$ are torques exerted on the body of the bacterium by the background shear flow and by the flagellum, respectively. Parameter ζ_r is the rotation drag coefficient, and $(1/\zeta_r)(T_{\text{shear}} + T_{\text{flagellum}})$ is the angular velocity of the body caused by shear and flagellum. It is well known [42] that T_{shear} can be explicitly written as a function of θ_0:

$$\begin{aligned} T_{\text{shear}} &= -\dot{\gamma}\zeta_r((1-\beta)\sin^2\theta_0 + \beta\cos^2\theta_0) \\ &= -\frac{\dot{\gamma}\zeta_r}{2}(1-(1-2\beta)\cos 2\theta_0). \end{aligned} \tag{2.6}$$

The equation $\zeta_r(d\theta_0/dt) = T_{\text{shear}}(\theta_0)$ is known as the Jeffery equation for rotating ellipses in shear flow [42,50]. To compute $T_{\text{flagellum}} = (\ell/2)N|_{s=0}$, one needs to solve the elasticity equations for the flagellum. However, using the asymptotic method as $\varepsilon \ll 1$, it is possible to represent $N|_{s=0}$ (and, thus, $T_{\text{flagellum}}$) as a function of θ_0, which results in a closed form of equation (2.5). The resulting equation is the same as the Jeffery equation for ellipses with the effective shape parameter $b = r\beta/(1+2r)$ in place of β. In other words, an ellipse with a rigid flagellum has the same trajectories as a more prolate ellipse with no flagellum. The equilibrium distribution which satisfies equation (2.5) for $\varepsilon \ll 1$ is given by

$$P(\theta_0) = \frac{q}{2\pi}\frac{1}{1-(1-2b)\cos(2\theta_0)}, \tag{2.7}$$

where constant $q = \sqrt{1-(1-2b)^2}$ is introduced, so $P(\theta_0)$ satisfies the normalization condition in (2.5). The effective viscosity is the suspension's time-independent property. Since solutions of equation (2.5) for $\varepsilon \ll 1$ converge to the equilibrium distribution (if one assumes a small rotational

Table 2. Main model parameters.

parameter	typical value	description
L	1.2×10^{-5} m	flagellum length
ℓ	0.5×10^{-5} m	body length (major axis of ellipse)
d	7×10^{-7} m	body thickness (minor axis of ellipse)
β	0.0162	body shape parameter, $\frac{d^2}{\ell^2+d^2}$
$\dot{\gamma}$	0.1 s^{-1}	shear rate
η_0	10^{-3} Pa s	viscosity of the surrounding fluid
F_p	10^{-7} N m^2	propulsion force
K_b	3×10^{-23} N m^2	flagellum bending stiffness
ζ_b	10^{-3} N s m^{-2}	drag coefficient per unit length for the flagellum
ζ_h	1.6×10^{-8} N s m^{-1}	drag coefficient for the body
ζ_r	6.7×10^{-20} N s m	rotational drag coefficient for the body
α	2	drag anisotropy factor
k_r	0.65	$L\zeta_b/\zeta_h$ (auxiliary parameter)
r	0.41	ℓ/L
ε	0.07	$L^4\dot{\gamma}\zeta_b/K_b$

diffusion), we use $P(\theta_0)$ from equation (2.7) when applying equation (2.1).

Substituting the asymptotic expansions into formula (2.1), the effective viscosity of the dilute suspension of flagellated swimmers is expressed as

$$\frac{\eta_{\text{eff}}-\eta_0}{\eta_0}=\Phi\frac{L^3}{\eta_0}Z_{\text{elastic}}(\beta,r)-\Phi\varepsilon\frac{F_pL^2}{\eta_0\dot{\gamma}}Z_{\text{prop}}(\beta,r), \qquad (2.8)$$

where Φ is the number density of bacteria in the suspension and expressions for the elastic and propulsion contributions, Z_{elastic} and Z_{prop}, can be found in electronic supplementary material, section 2.5; both Z_{elastic} and Z_{prop} are positive. Equation (2.8) implies that the change of the effective viscosity is obtained by the interplay between elastic and propulsion contributions. Namely, whatever the parameters β and r are, the propulsion decreases the viscosity, whereas the elastic part of the stress tends to increase the viscosity (figure 2). For small r (i.e. long flagella), Z_{prop} behaves as $1/r^5$ whereas Z_{elastic} behaves as $1/(r^2\log(r))$. This implies that for r small enough, the propulsion should dominate elasticity.

2.1.3. Numerical study

We performed computational analysis of MMFS and computed the effective viscosity η_{eff} as well as propulsion and elastic contributions $\eta_{\text{propulsion}}$ and η_{elastic}. The expected value integral in the r.h.s of equation (2.1) was approximated by the time average of its integrand.

For large K_b (small ε), the results of the numerical solution are in a good agreement with asymptotic expression equation (2.8) (figure 2 and table 1). Note that the asymptotic parameter ε is proportional to L^4, so the agreement between numerical and asymptotic solutions is lost for small r (long flagellum). The set of values of the flagellum length L for which the decrease in viscosity is observed depends on the bending stiffness K_b. Table 1 compares results of asymptotic approach and numerical solution; the threshold values of L, r and ε required for a decrease of viscosity are given.

For the following model parameters: $K_b=3\times10^{-23}$ N m^2, $\eta_0=10^{-3}$ Pa s, $L=12$ µm and $F_p=1.5$ µN m^{-1}; asymptotic and numerical values of η_{eff} are in agreement with experiment [9], i.e. we predict a decrease in effective viscosity of $\approx$10% for the number density of $\Phi=5\times10^9$ cm^{-3} (see the part $\Phi<10^9$ cm^{-3} of fig. 3 in [9]). The overall viscosity reduction is somewhat smaller than observed experimentally. It was shown that multiple physical factors may contribute to the viscosity reductions, including long-range hydrodynamic interactions between the bacteria [51], curvature of the flow streamlines [19] and tumbling [29].

Certain flagellated bacteria have the ability to swim through environments of relatively high viscosity [52–54]. Moreover, the bacteria maintain an almost constant speed independent from the fluid resistance they encounter. In the first approximation, the velocity of bacteria is $\sim F_p/\eta_0$. Therefore, bacteria increase their propulsion force while surrounded by a more viscous fluid. In such a fluid ($\eta_0=5.10^{-3}$ Pa s and $F_p=1.5$ µN m^{-1}), we predict a decrease of viscosity for $r<0.55$ ($r=0.5$ for *B. subtilis*) (figure 2*c*). For higher β values, the decrease of effective viscosity also occurs for shorter flagella (figure 2*d*).

2.2. Flagellated swimmers can escape from the wall

Here, we consider how flagellar flexibility assists a bacterium to escape from the wall. A swimmer can be entrapped by a wall such that its orientation is perpendicular to the wall. This kind of entrapment may happen, for example, in lyotropic (water soluble) nematic liquid crystal with the homeotropic surface anchoring [38,40] (the liquid crystal director is perpendicular to the wall). Since the bacteria tend to align with the nematic director, they eventually become perpendicular to the wall (for simplicity we neglect here the effects associated with the anisotropic elastic and viscous torques exerted by the liquid crystal on a bacterium). Moreover, motile bacteria would hit the wall. However, due to flagella rotation and bending, this perpendicular alignment may become unstable.

Settings of the problem are as follows. The bacterium's body initially has the orientation $\theta_0=\pi$, that is, the body is oriented horizontally, pointing to the right, at the vertical wall $x=0$. The flagella is initially slightly perturbed from a straight configuration (while unstable, perfectly straight flagella will lead to no motion). The bacterium's body experiences three torques: (i) due to the flagella, applied at the point of its attachment to the body, (ii) due to the wall, applied at

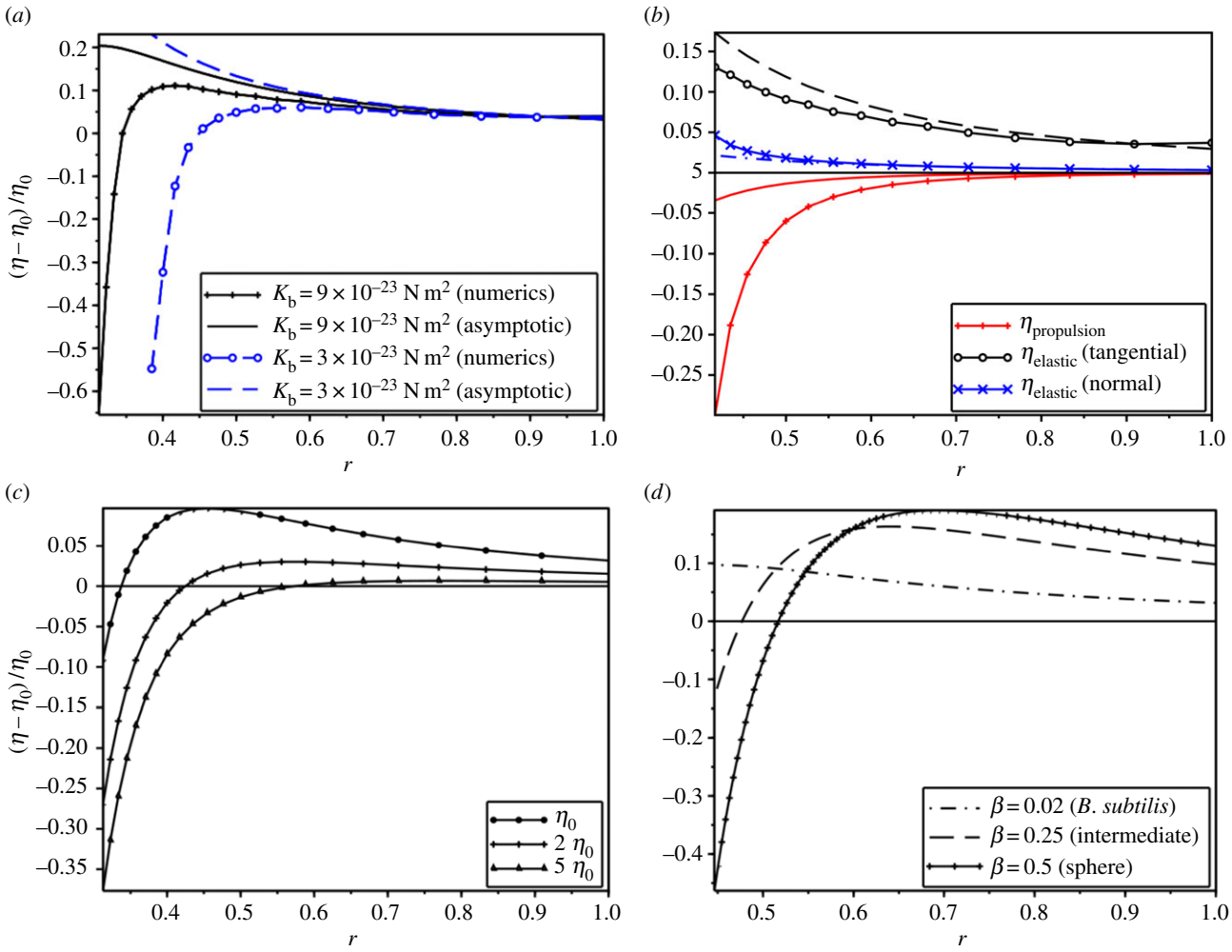

Figure 2. Effective viscosity as a function of model parameters. (*a*) Comparison of the effective viscosity change obtained by two scale asymptotic expansions and numerical simulations for $K_b = 9\times10^{-23}$ N m^2 (black) and $K_b = 3\times10^{-23}$ N m^2 (blue) and various r. (*b*) Contributions (scaled by η_0) from propulsion and elasticity (both tangential and normal components) for $K_b = 3\times10^{-23}$ N m^2 are shown. (*c*) Effective viscosity η_{eff} for various bulk viscosities η_0. (*d*) Effective viscosity η_{eff} versus r for various body shape constants β. (Online version in colour.)

the point of touching the wall (if the body does not touch the wall, then this torque is 0) and (iii) due to the surrounding viscous fluid (figure 3*a*).

We use MMFS with a modification to take into account the additional torque when the swimmer is touching the wall. A variety of non-trivial dynamic regimes was numerically observed depending on the values of the bending stiffness of the flagellum, K_b, all other parameters being fixed; their values can be found in table 2. Numerical analysis shows that qualitative behaviour of the swimmer depends on the bending stiffness of the flagellum, K_b. If $K_b < 5\times10^{-24}$ N m^2 (relatively 'soft' flagellum), the swimmer rotates and swims parallel to the wall. Thus, in this case, though the swimmer is not immobilized at the wall, it is still entrapped by the wall and cannot escape. For bending stiffness in the range of 5×10^{-24} N m^2 $< K_b <$ 2.2×10^{-23} N m^2, the swimmer eventually swims away from the wall, hence showing the ability to escape due to the flagellum. However, in the range 1.5×10^{-24} N m^2 $< K_b <$ 9.1×10^{-24} N m^2 (pink interval in the centre in figure 3*b*), the swimmer escapes from the wall but keeps turning due to non-zero N_0, eventually reorients against the wall, hits it, escapes again, turns around, hits the wall again, etc. In other words, the swimmer executes loops at the wall. In this case, we count that the swimmer is trapped. For the large bending stiffness, $K_b > 2.2\times10^{-23}$ N m^2 ('almost rigid' flagellum), as is expected for the rigid flagellum, the swimmer rotates by $\pi/2$ and then swims parallel to the wall (figure 3*b*,*c*; electronic supplementary material, videos S1–S4). The difference between 'soft' and 'almost rigid' cases is that for a 'soft' flagellum the body exhibits visible oscillations due to buckling instability, whereas in the other case, it swims straight, parallel to the wall. This non-trivial qualitative behaviour of the swimmer depending on K_b is also observable when no obstacle is present in the fluid. Regardless of initial flagella shape the swimmer eventually either orients itself towards a certain direction and swims straight or exhibits periodic oscillations (figure 3*d*) for the case with no background flow; more complicated dependence on K_b of the large time behaviour of the swimmer was observed in Poiseuille flow; see fig. 3(e) in [27]; see also electronic supplementary material, video S5). These differences in qualitative behaviour may serve as a basis to isolate bacteria with bending stiffness in a given range (or equivalently, different numbers of flagella since effective K_b is proportional to the number of flagella).

3. Discussion

We provide a heuristic explanation why the flagellum helps decrease the viscosity. For the illustration, we will use the

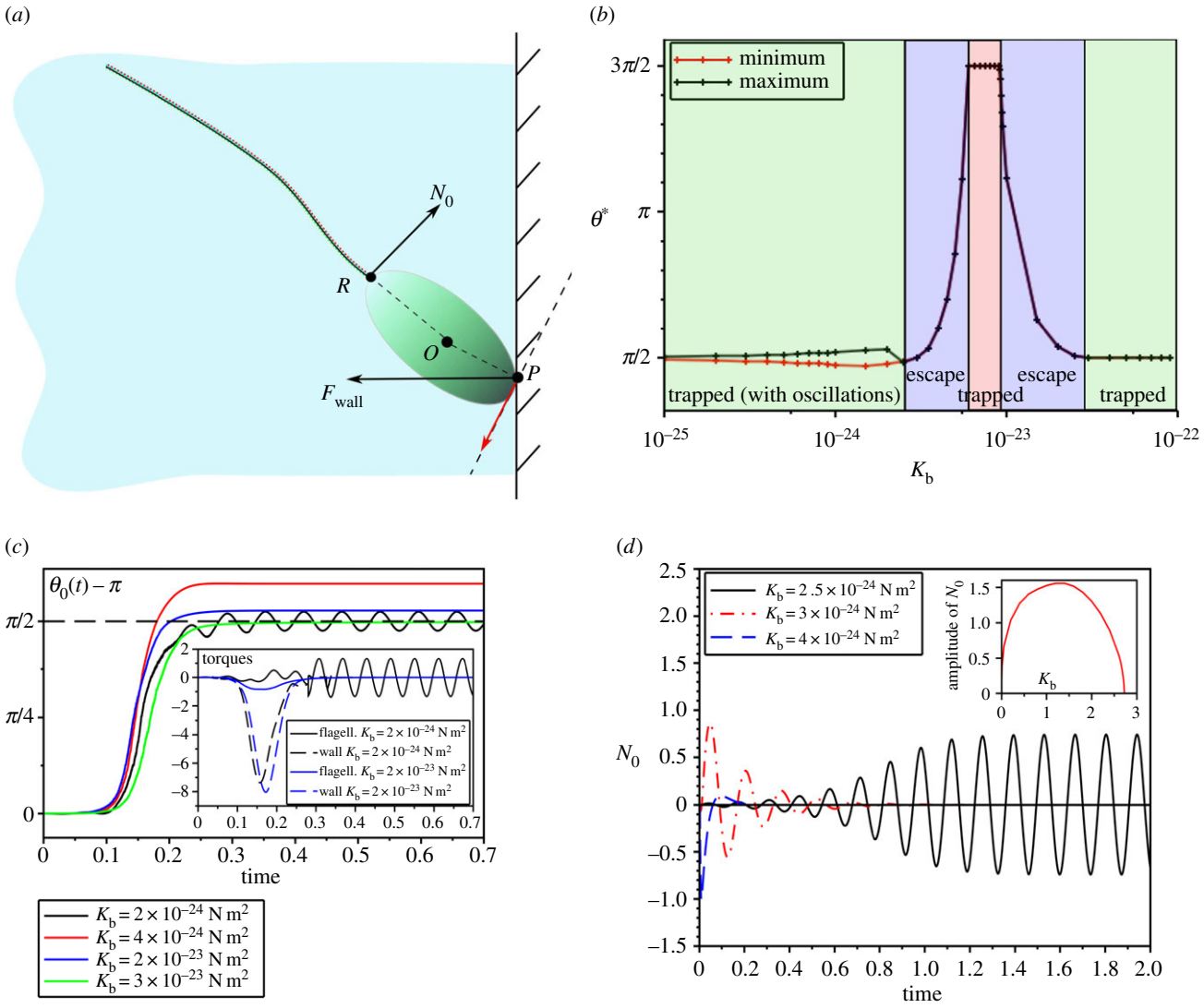

Figure 3. Escape from the wall. (*a*) Bacteria at the wall (sketch). Body is an ellipse centred at point *O*; the body touches the wall at point *P*; the flagellum is rigidly attached to the body at point *R*. Three forces act on the body: the normal force coming from the flagellum N_0, the wall reaction F_{wall} and the fluid over the boundary of the ellipse. Red arrow stands for the component of F_{wall} contributing to the torque. The light blue zone represents the domain with fluid. (*b*) The plot demonstrates how qualitative behaviour of an initially entrapped swimmer depends on bending stiffness of the flagellum K_b: the swimmer either remains trapped (red and green zones), or eventually escapes with a limiting angle from $(\pi/2, 3\pi/2)$ (blue zone); θ^* (vertical axis) denotes the orientation of the swimmer for large times, $t \gg 1$. (*c*) Evolution of the orientation angle (main plot) and torques due to the flagellum and the wall (inset). A bacterium swims towards the wall and touches it at time $t \approx 0.1$. When the body of the bacterium touches the wall, the torque due to the wall becomes non-zero. (*d*) The plot depicts dynamics N_0 for various K_b of the swimmer in the fluid with no obstacles and no background flow (the plot for $K_b = 4\times10^{-24}$ N m^2 is magnified by a factor 200 for better visibility); three plots demonstrate that depending on K_b the swimmer eventually exhibits oscillations with constant or decaying amplitude or N_0 converges to 0 with no oscillations. Inset: the plot demonstrates the dependence on K_b of the amplitude of N_0 when the swimmer exhibits oscillations. (Online version in colour.)

force dipole representation of a bacterium, that is, the representation by two forces of equal magnitude and opposite directions. In [4], it was shown experimentally that the flow from a swimming bacterium is well approximated by the flow generated by a force dipole. Above we mentioned that such a representation is not sufficient for our purposes to study the impact of flexible flagellum. However, for the sake of simplicity the force dipole model is sufficient if we allow the dipole not to be straight: the line connecting points where two opposite forces are exerted is not necessarily parallel to these forces (figure 4*b*).

In the case of straight dipoles, that is, when the flagellum is rigid and straight, swimmers with orientations $\theta_0 = \pi/4$ or $\theta_0 = 5\pi/4$ enhance the fluid flow, whereas swimmers with orientations $\theta_0 = 3\pi/4$ or $\theta_0 = 7\pi/4$ decrease the fluid flow (figure 4*a*). The symmetry in the body orientation distribution does not change the viscosity. The flexibility of the flagellum breaks the symmetry in the dipole orientation distribution (figure 4*b*). Thus, owing to the flagellar bending, a bacterial body oriented at either $\pi/2$ or $3\pi/2$ (neutral for η_{eff} if the flagellum is straight) creates a force dipole oriented close to $7\pi/4$ or $\pi/4$, respectively. As a result, on average, the orientations helping the fluid to flow, and thus to increase the background shear, are more likely than other orientations, and, therefore, the viscosity is decreased if the flagellum can bend.

In contrast with [43], the propulsion contribution to η_{eff} has no apparent singularity for the strain rate $\dot{\gamma} = 0$ (which is regularized by an infinitesimal rotational diffusion), and in the first approximation (rigid flagellum) it does not depend on the shear rate. This singularity is regularized because ε is proportional to $1/\dot{\gamma}$. The bulk stress depends on how much the flagellum bends, which is in the first approximation directly proportional to the bulk rate of strain. As a

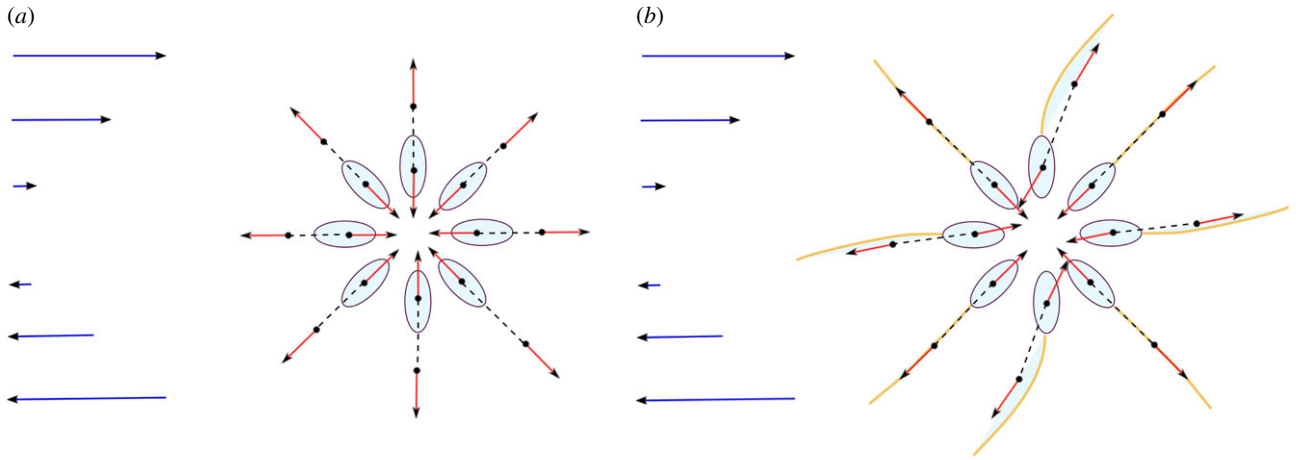

Figure 4. Illustration of the viscosity reduction due to flagellar bending. Force dipole (red arrows) exerted by the swimmer on the fluid, for different body orientations $i\pi/4$, $i = 0, \ldots, 7$. Blue arrows illustrate background shear flow. (*a*) Swimmers with a rigid flagellum: orientation of the bacterial body coincides with the orientation of the force dipole. (*b*) Swimmers with a flexible flagellum: orientation of the force dipole differs from the orientation of the swimmer and the corresponding force dipole amplifies the background shear flow. (Online version in colour.)

result, the shear rate modifies linearly the propulsion stress; then their ratio is constant in $\dot{\gamma}$: as $\dot{\gamma} \to 0$ (and, thus, $\varepsilon \to 0$), the propulsion contribution to the effective viscosity equals $-\Phi(L^6\zeta_b F_p/K_b)Z_{\text{prop}}(\beta, r)$. Thus, the small strain rate $\dot{\gamma}$ limit is well defined, and leads to a specific value of the effective viscosity even in the absence of fluctuations. This result is in agreement with the experiment [11] where a well-defined value of effective viscosity was observed for small shear rates.

4. Conclusion

In this work, we demonstrated how the flexibility of bacterial flagella affects macroscopic properties of suspension of microswimmers. We found that flagellar bending may lead to a decrease of the effective viscosity in the absence of random reorientations. This effect is amplified with the increase of the viscosity of the suspending fluid since many bacteria often increase their propulsion force [52–54]. Moreover, we showed that flagella buckling may assist bacteria to escape entrapment at the wall. Our findings highlight the wealth of new intriguing phenomena stemming from the flexibility of the swimmer's body that include reduction in the viscosity, escape from the wall entrapment, migration towards the flow centre line and many others.

Here, we approximated helical flagella by an elastic beam with the propulsion force distributed uniformly along the beam. Obviously, this approximation neglects intrinsic chirality of the flagellum, which leads to its clockwise rotation and counter-clockwise rotation of the head. The chirality of the flagellum can be responsible for such phenomena as rheotaxis [18] and circular motion near the wall [34]. Incorporating flagellar chirality into our analysis would be desirable, but technically challenging. We anticipate that the torques arising from the helical shape of the flagellum are negligible compared with the bending stresses considered here, and, thus, do not affect the phenomena considered in this work (see electronic supplementary material, section 3). While these torques are small, on a long time scale they can possibly result in more complex near-wall three-dimensional trajectories. For example, looping motion in the direction perpendicular to the wall can be combined with in-plane circular motion.

5. Material and methods

As mentioned at the end of §1, in this work, we extend the model from [27] which is abbreviated as MMFS. Given the initial state of the swimmer (orientation of the body and the shape of the flagellum at time $t = 0$), MMFS entirely determines the state of the swimmer for all times $t > 0$. The unknown quantities of MMFS are the orientation of the body $\theta_0(t)$, the elastic stress of the flagellum $Q(s,t)$, and the tangential angle $\theta(s, t)$ of the flagellum at the point corresponding to arclength parameter s; $s = 0$ is at the body/flagellum interface and $s = L$ is at the free end of the flagellum. Using basic geometric formulas, given $Q(s, t)$, $\theta(s, t)$ and $\theta_0(t)$, one can recover the trajectory of the swimmer, the shape and the location of every point of the flagellum $X(s, t) = (x(s, t), y(s, t))$. MMFS requires solving a coupled system of an ordinary differential equation for $\theta_0(t)$ and partial differential equations for $\theta(s, t)$ and $Q(s, t)$. Electronic supplementary material, S1, contains the full description of MMFS.

The underlying physical assumptions of MMFS are the following: (i) the two-dimensional swimmer is composed of a rigid ellipse (body) and a flexible one-dimensional segment (flagellum) of length L; the flagellum is rigidly attached to the body (clamped); (ii) elastic and propulsion forces on the flagellum generate the thrust force which balances the drag force and leads to the motion of the swimmer; (iii) a propulsion force is uniformly distributed along the flagellum; and (iv) background flow is not modified by the flagellum. The shape of the body (which is an ellipse) is described by parameter $\beta = d^2/(\ell^2 + d^2)$ where ℓ and d are the major and minor axes, respectively. Small β corresponds to rod-like bodies, and $\beta = \frac{1}{2}$ corresponds to spheres. The full list of model parameters as well as their typical values can be found in table 2.

We stress here that a bacterial flagellum is a flexible helical filament which exhibits propeller-like motion by rotating around its helical axis, and these rotations generate the propulsion force. In MMFS, according to (ii) above, this corresponds to the thrust force having two separate components: due to flagellar bending (the elastic force) and due to the propulsion mechanism (the propulsion force). Moreover, flagellar bundle is modelled as a one-dimensional (curved) segment in a plane with no helical structure, since the propulsion force already takes into account the helical structure of the flagellum and its axial rotation. These approximations are needed to make the model tractable analytically. We show in this work that despite these simplifications MMFS captures important phenomenology: viscosity reduction and escape from the wall. We model peritrichously flagellated bacteria (such as *Bacillus subtilis*) and

the one-dimensional curve segment represents not a single flagellum but a flagellar bundle in which each flagellum is connected to a body by the hook, which is more flexible than the flagellum. These very short hooks (with the length of about only 50 nm) are randomly distributed along the bacterial body, and the clamped boundary conditions effectively replace the hooks and individual flagellar filaments before they assemble in a single bundle. For a computational model that takes into account a flexible hook explicitly, we refer to [55]. A somewhat similar approach was considered in [56] to study magneto-elastic filaments.

Data accessibility. The datasets supporting this article have been uploaded as part of the electronic supplementary material.

Author's contributions. M.P., M.T., L.B. and I.S.A. designed and performed the study and wrote the paper. M.P. and M.T. contributed equally to this work.

Competing interests. The authors declare that they have no competing financial interests.

Acknowledgments. The work of M.T., M.P. and L.B. was supported by NIH grant no. 1R01GM104978-01. The research of I.S.A. was supported by the US Department of Energy (DOE), Office of Science, Basic Energy Sciences (BES), Materials Science and Engineering Division.

References

1. Wu XL, Libchaber A. 2000 Particle diffusion in a quasi-two-dimensional bacterial bath. *Phys. Rev. Lett.* **84**, 3017–3020. (doi:10.1103/PhysRevLett.84.3017)
2. Dombrowski C, Cisneros L, Chatkaew S, Goldstein RE, Kessler JO. 2004 Self-concentration and large-scale coherence in bacterial dynamics. *Phys. Rev. Lett.* **93**, 098103. (doi:10.1103/PhysRevLett.93.098103)
3. Sokolov A, Aranson I, Kessler J, Goldstein R. 2007 Concentration dependence of the collective dynamics of swimming bacteria. *Phys. Rev. Lett.* **98**, 158102. (doi:10.1103/PhysRevLett.98.158102)
4. Drecher K, Dunkel J, Cisneros L, Ganguly S, Goldstein R. 2011 Fluid dynamics and noise in bacterial cell-cell and cell-surface scattering. *Proc. Natl Acad. Sci. USA* **108**, 10 940–10 945. (doi:10.1073/pnas.1019079108)
5. Rusconi R, Guasto JS, Stocker R. 2014 Bacterial transport suppressed by fluid shear. *Nat. Phys.* **10**, 212–217. (doi:10.1038/nphys2883)
6. Stocker R. 2012 Marine microbes see a sea of gradients. *Science* **338**, 628–633. (doi:10.1126/science.1208929)
7. Wensink HH, Dunkel J, Heidenreich S, Drescher K, Goldstein RE, Löwen H, Yeomans JM. 2012 Meso-scale turbulence in living fluids. *Proc. Natl Acad. Sci. USA* **109**, 14 308–14 313. (doi:10.1073/pnas.1202032109)
8. Sokolov A, Aranson IS. 2012 Physical properties of collective motion in suspensions of bacteria. *Phys. Rev. Lett.* **109**, 248109. (doi:10.1103/PhysRevLett.109.248109)
9. Sokolov A, Aranson IS. 2009 Reduction of viscosity in suspension of swimming bacteria. *Phys. Rev. Lett.* **103**, 148101. (doi:10.1103/PhysRevLett.103.148101)
10. Gachelin J, Miño G, Berthet H, Lindner A, Rousselet A, Clément E. 2013 Non-newtonian viscosity of *Escherichia coli* suspensions. *Phys. Rev. Lett.* **110**, 268103. (doi:10.1103/PhysRevLett.110.268103)
11. López H, Gachelin J, Douarche C, Auradou H, Clément E. 2015 Turning bacteria suspensions into superfluids. *Phys. Rev. Lett.* **115**, 028301. (doi:10.1103/PhysRevLett.115.028301)
12. Sokolov A, Apodaca MM, Grzybowski BA, Aranson IS. 2009 Swimming bacteria power microscopic gears. *Proc. Natl Acad. Sci. USA* **107**, 969–974. (doi:10.1073/pnas.0913015107)
13. Di Leonardo R *et al.*. 2010 Bacterial ratchet motors. *Proc. Natl Acad. Sci. USA* **107**, 9541–9545. (doi:10.1073/pnas.0910426107)
14. Kaiser A, Peshkov A, Sokolov A, ten Hagen B, Löwen H, Aranson IS. 2014 Transport powered by bacterial turbulence. *Phys. Rev. Lett.* **112**, 158101. (doi:10.1103/PhysRevLett.112.158101)
15. Sokolov A, Goldstein R, Feldchtein F, Aranson I. 2009 Enhanced mixing and spatial instability in concentrated bacterial suspensions. *Phys. Rev. E* **80**, 031903. (doi:10.1103/PhysRevE.80.031903)
16. Pushkin DO, Yeomans JM. 2014 Stirring by swimmers in confined microenvironments. *J. Stat. Mech. Theory Exp.* **2014**, P04030. (doi:10.1088/1742-5468/2014/04/P04030)
17. Ariel G, Rabani A, Benisty S, Partridge JD, Harshey RM, Be'er A. 2015 Swarming bacteria migrate by Lévy Walk. *Nat. Commun.* **6**, 8396. (doi:10.1038/ncomms9396)
18. Marcos M, Fu HC, Powers TR, Stocker R. 2012 Bacterial rheotaxis. *Proc. Natl Acad. Sci. USA* **109**, 4780–4785. (doi:10.1073/pnas.1120955109)
19. Sokolov A, Aranson IS. 2016 Rapid expulsion of microswimmers by a vortical flow. *Nat. Commun.* **7**, 1114. (doi:10.1038/ncomms11114)
20. Son K, Guasto J, Stocker R. 2013 Bacteria can exploit a flagellar buckling instability to change direction. *Nat. Phys.* **9**, 494–498. (doi:10.1038/nphys2676)
21. Vogel R, Stark H. 2012 Motor-driven bacterial flagella and buckling instabilities. *Eur. Phys. J. E* **35**, 15. (doi:10.1140/epje/i2012-12015-0)
22. Vogel R, Stark H. 2013 Rotation-induced polymorphic transitions in bacterial flagella. *Phys. Rev. Lett.* **110**, 158104. (doi:10.1103/PhysRevLett.110.158104)
23. Brumley D, Rusconi R, Son K, Stocker R. 2015 Flagella, flexibility and flow: physical processes in microbial ecology. *Eur. Phys. J.* **224**, 3119–3140. (doi:10.1140/epjst/e2015-50138-9)
24. Zöttl A, Stark H. 2012 Nonlinear dynamics of a microswimmer in Poiseuille flow. *Phys. Rev. Lett.* **108**, 218104. (doi:10.1103/PhysRevLett.108.218104)
25. Zöttl A, Stark H. 2013 Periodic and quasiperiodic motion of an elongated microswimmer in Poiseuille flow. *Eur. Phys. J. E* **36**, 1. (doi:10.1140/epje/i2013-13001-8)
26. Adhyapak TC, Stark H. 2015 Zipping and entanglement in flagellar bundle of *E. coli*: role of motile cell body. *Phys. Rev. E* **92**, 052701. (doi:10.1103/PhysRevE.92.052701)
27. Tournus M, Kirshtein A, Berlyand L, Aranson I. 2015 Flexibility of bacterial flagella in external shear results in complex swimming trajectories. *J. R. Soc. Interface* **12**, 20140904. (doi:10.1098/rsif.2014.0904)
28. Haines B, Aranson I, Berlyand L, Karpeev D. 2008 Effective viscosity of dilute bacterial suspensions: a two-dimensional model. *Phys. Biol.* **5**, 046003. (doi:10.1088/1478-3975/5/4/046003)
29. Haines B, Sokolov A, Aranson I, Berlyand L, Karpeev D. 2009 Three-dimensional model for the effective viscosity of bacterial suspensions. *Phys. Rev. E* **80**, 041922. (doi:10.1103/PhysRevE.80.041922)
30. Saintillan D. 2010 Extensional rheology of active suspensions. *Phys. Rev. E* **81**, 056307. (doi:10.1103/PhysRevE.81.056307)
31. Berke A, Turner L, Berg H, Lauga E. 2008 Hydrodynamic attraction of swinning microorganisms by surfaces. *Phys. Rev. Lett.* **101**, 038102. (doi:10.1103/PhysRevLett.101.038102)
32. Rothschild L. 1963 Non-random distribution of bull spermatozoa in a drop of sperm suspension. *Nature* **198**, 1221. (doi:10.1038/1981221a0)
33. Berg H, Turner L. 1990 Chemotaxis of bacteria in glass capillary arrays. *Escherichia coli*, motility, microchannel plate, and light scattering. *Biophys. J.* **58**, 919–930. (doi:10.1016/S0006-3495(90)82436-X)
34. DiLuzio WR, Turner L, Mayer M, Garstecki P, Weibel DB, Berg HC, Whitesides GM. 2005 *Escherichia coli* swim on the right-hand side. *Nature* **435**, 1271–1274. (doi:10.1038/nature03660)
35. Ramia M, Tullock D, Phan-Thien N. 1993 The role of hydrodynamic interaction in the locomotion of microorganisms. *Biophys. J.* **65**, 755–778. (doi:10.1016/S0006-3495(93)81129-9).
36. Frymier P, Ford R, Berg H, Cummings P. 1995 Three-dimensional tracking of motile bacteria near a solid planar surface. *Proc. Natl Acad. Sci. USA* **92**, 6195–6199. (doi:10.1073/pnas.92.13.6195)
37. Vigeant M, Ford R, Wagner M, Tamm L. 2002 Reversible and irreversible adhesion of motile *Escherichia coli* cells analyzed by total internal reflection aqueous fluorescence microscopy. *Appl. Environ. Microbiol.* **68**, 2794–2801. (doi:10.1128/AEM.68.6.2794-2801.2002)
38. Mushenheim P, Trivedi R, Roy S, Arnold M, Weibel D, Abbott N. 2015 Effects of confinement, surface-

induced orientations and strain on dynamical behaviors of bacteria in thin liquid crystalline films. *Soft Matter* **11**, 6821–6831. (doi:10.1039/C5SM01489A)

39. Zhou S, Sokolov A, Lavrentovich OD, Aranson IS. 2014 Living liquid crystals. *Proc. Natl Acad. Sci. USA* **111**, 1265–1270. (doi:10.1073/pnas.1321926111)
40. Zhou S, Tovkach O, Golovaty D, Sokolov A, Aranson IS, Lavrentovich OD. 2017 Dynamic states of swimming bacteria in a nematic liquid crystal cell with homeotropic alignment. *New J. Phys.* **19**, 055006. (doi:10.1088/1367-2630/aa695b)
41. Batchelor G. 1967 *An introduction to fluid dynamics*. Cambridge, UK: Cambridge University Press.
42. Kim S, Karrila J. 1991 *Microhydrodynamics: principles and selected applications*. New York, NY: Dover.
43. Ryan S, Haines B, Berlyand L, Ziebert F, Aranson I. 2011 Viscosity of bacterial suspensions: hydrodynamic interactions and self-induced noise. *Phys. Rev. E* **83**, 050904. (doi:10.1103/PhysRevE.83.050904)
44. Batchelor G. 1970 The stress system in a suspension of force-free particles. *J. Fluid Mech.* **41**, 545–570. (doi:10.1017/S0022112070000745)
45. Fürthauer S, Strempel M, Grill S, Jülicher F. 2012 Active chiral fluids. *Eur. Phys. J. E* **35**, 89. (doi:10.1140/epje/i2012-12089-6)
46. Kirkwood J, Auer P. 1951 The visco-elastic properties of solutions of rod-like macromolecules. *J. Chem. Phys.* **19**, 281–283. (doi:10.1063/1.1748194)
47. Doi M, Edwards S. 1988 *The theory of polymer dynamics*. Oxford, UK: Oxford University Press.
48. Ziebert F, Aranson I. 2008 Rheological and structural properties of dilute active filament solutions. *Phys. Rev. E* **77**, 011918. (doi:10.1103/PhysRevE.77.011918)
49. Einstein A. 1906 Eine neue bestimmung der moleküldimensionen. *Ann. Phys.* **324**, 289–206. (doi:10.1002/andp.19063240204)
50. Jeffery G. 1922 The motion of ellipsoidal particles immersed in a viscous fluid. *Proc. R. Soc. Lond. A* **102**, 161–179. (doi:10.1098/rspa.1922.0078)
51. Ryan SD, Haines BM, Berlyand L, Ziebert F, Aranson IS. 2011 Viscosity of bacterial suspensions: hydrodynamic interactions and self-induced noise. *Phys. Rev. E* **83**, 050904. (doi:10.1103/PhysRevE.83.050904)
52. Greenberg E, Canale-Parola E. 1977 Motility of flagellated bacteria in viscous environments. *J. Bacteriol.* **132**, 356–358.
53. Schneider W, Doetsch R. 1974 Effect of viscosity on bacterial motility. *J. Bacteriol.* **117**, 696–701.
54. Keller J. 1974 Effect of viscosity on swimming velocity of bacteria. *Proc. Natl Acad. Sci. USA* **71**, 3253–3254. (doi:10.1073/pnas.71.8.3253)
55. Shum H, Gaffney EA. 2012 The effects of flagellar hook compliance on motility of monotrichous bacteria: a modeling study. *Phys. Fluids* **24**, 061901. (doi:10.1063/1.4721416)
56. Roper M, Dreyfus R, Baudry J, Fermigier M, Bibetter J, Stone H. 2006 On the dynamics of magnetically driven elastic filaments. *J. Fluid Mech.* **554**, 167–190. (doi:10.1017/S0022112006009049)